authors' knowledge. Such a detailed theory would be a formidable task but would probably be quite rewarding.

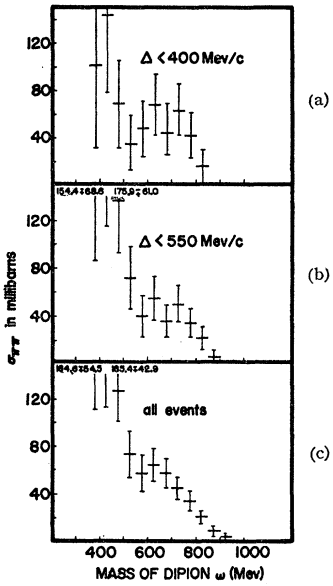

FIG. 18. Pion-pion interaction cross section for $\pi^- - \pi^0$ from $\pi^- + p \to \pi^- + \pi^0 + p$ events. The cross section has been calculated (a) from events with $\Delta < 400$ Mev/c, (b) from events with $\Delta < 550$ Mev/c, and (c) from all events.

VIII. ACKNOWLEDGMENTS

The pictures for this experiment were made available to us by Professor J. Steinberger and the Columbia Bubble Chamber Group. Their generosity is gratefully acknowledged. Dr. M. Schwartz and Dr. R. Plano kindly supplied details of the chamber and of the exposure.

Mrs. R. P. Chen did much of the scanning and measurement involved in the project.

Dr. R. M. Steinheimer kindly calculated the basic momentum spectra at 1.3 Bev for use in the analysis.

The help of the Numerical Analysis Laboratory at the University of Wisconsin and the Computing Center at the University of Kentucky in providing computing facilities and auxiliary equipment for the analysis was indispensible.

One of the authors (WDS) was aided by a National Science Foundation grant at the University of Kentucky during the latter stages of the work.

Helpful discussions with Dr. V. P. Kenney are acknowledged by WDS.

PHYSICAL REVIEW VOLUME 126, NUMBER 1 APRIL 1, 1962

Positive-Pion Cross Sections on Complex Nuclei*

JOHN C. CARIS,† EDWARD A. KNAPP,‡ VICTOR PEREZ-MENDEZ, AND WALTON A. PERKINS§
Lawrence Radiation Laboratory, University of California, Berkeley, California

(Received July 10, 1961)

Absorption and diffraction cross sections were measured for positive pions at a kinetic energy of 442 Mev. The target elements used were C, Al, Cu, and Cd. The absorption and diffraction cross sections were determined by fitting the experimental data (taken at six angles) to the shape given by the optical-model theory. The nuclear radius and the falloff parameter were taken to be approximately those determined from nuclear charge distribution measurements. The experimental data are compared with the results of the optical-model theory. Experimental values for the imaginary part of the potential V_I are in agreement with the theoretical value. However, the experimental values for the real potential V_R increase with increasing atomic number, becoming far larger than the theoretical value.

I. INTRODUCTION

MEASUREMENTS of total and absorption cross sections of pions in nuclei can be used to obtain information both on nuclear structure and on the pion-nucleon interactions. The theoretical interpretation of measurements of this sort is usually done using some form of an optical-model theory, as originally proposed by Fernbach, Serber, and Taylor[1] and since extended by many authors.[2,3]

Nuclear properties which can be deduced by experiments of this kind are the size and density distribution of nuclei. Analogous information on the charge distribution in nuclei has been obtained to a high degree of accuracy from the electron scattering experiments of

* This work was performed under auspices of the U. S. Atomic Energy Commission.

† Present address: Experimental Station, Polychemicals Department, E. I. du Pont de Nemours & Company, Wilmington, Delaware.

‡ Present address: Los Alamos Scientific Laboratory, University of California, Los Alamos, New Mexico.

§ Lawrence Radiation Laboratory, University of California, Livermore, California.

[1] S. Fernbach, R. Serber, and T. B. Taylor, Phys. Rev. **75**, 1352 (1949).

[2] K. M. Watson, Phys. Rev. **89**, 575 (1953); W. W. Wada, *ibid.* **92**, 152 (1953); N. C. Francis and K. M. Watson, *ibid.* **92**, 291 (1953); G. Takeda and K. M. Watson, *ibid.* **97**, 1336 (1955); L. S. Kisslinger, *ibid.* **98**, 768 (1955); R. M. Frank, J. L. Gammel, and K. M. Watson, *ibid.* **101**, 891 (1956); K. M. Watson, *ibid.* **105**, 1388 (1957).

[3] K. M. Watson and C. Zemach, Nuovo cimento **10**, 452 (1958),

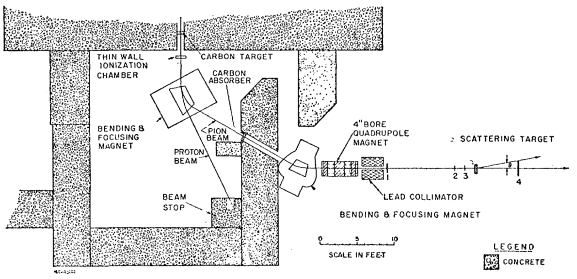

FIG. 1. Experimental arrangement.

Hofstadter and co-workers at Stanford University.[4] If we adopt the point of view that the distribution of nuclear matter in nuclei is approximately the same as the charge distribution, then the nuclear radius and the falloff parameter are assumed to be known. With these two parameters determined by other means, the pion-nucleus cross sections furnish a more direct evaluation of the optical-model potentials.

On the basis of general quantum-mechanical principles, the magnitude of the optical potentials can be related to the real and imaginary parts of the forward scattering amplitudes of the elementary pion-nucleon interaction. The imaginary part is given by the optical theorem $\mathrm{Im}f(0)=\sigma_T/4\pi\lambda$, where σ_T is the pion-nucleon total cross section. The real part, $\mathrm{Re}f(0)$, can be obtained from the measured values of σ_T as a function of energy by use of dispersion theory.

The measurements of pion-nucleus cross sections permit evaluation of the real and imaginary parts of the optical potentials. These potentials can also be calculated from the more elementary pion-nucleon cross sections if certain assumptions are made.[3] Consistency of the two sets of optical potentials then tests the validity of the assumptions made.

In the present experiment the total and absorption cross sections for positive pions incident on C, Al, Cu, and Cd targets were measured at an energy of 442 ± 8 Mev. These target nuclei were chosen to obtain data over a wide range of nuclear radii. An upper limit on the Z of the target nucleus was set by the requirement that multiple Coulomb corrections to the data be small enough to be adequately treated. The energy of the incident pions in the experiment was chosen as 442 Mev, since it was known from previous data[5] that in this energy region the magnitude of the real part of the forward scattering amplitude is considerably larger than the imaginary part and is, therefore, the major contributor to that amplitude. Data in the energy region of 442 Mev are thus more sensitive to predictions of dispersion theory and of its relation to the optical model.

[4] R. Hofstadter, Revs. Modern Phys. **28**, 214 (1956); R. Hofstadter, Ann. Rev. Nuclear Sci. **7**, 231 (1957).

[5] R. L. Cool, O. Piccioni, and D. Clark, Phys. Rev. **103**, 1082 (1956); J. W. Cronin, Phys. Rev. **118**, 824 (1960).

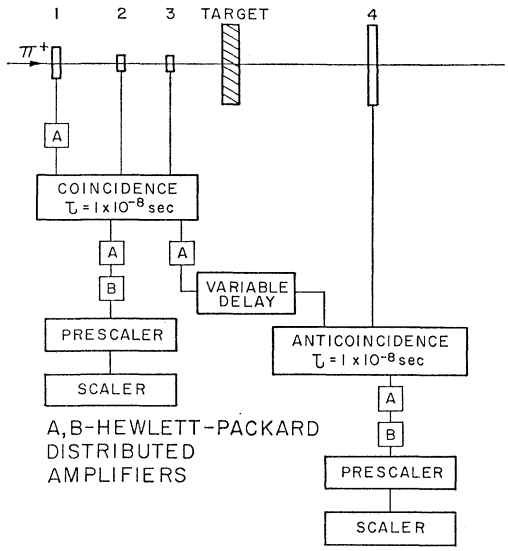

FIG. 2. Block diagram of the electronics used for monitoring beam and for counting particles scattered at an angle greater than θ.

II. EXPERIMENTAL ARRANGEMENT

A. Experimental Procedure

The experimental arrangement is shown in Fig. 1. The total cross sections for pions were measured by an attenuation experiment in good and poor geometry. By cycling short runs of C, Al, blank, Cu, and Cd targets at each distance, we minimized the effect of possible slow electronic drifts. Actually no detectable drifts occurred during the run.

The position of counter 4 (the transmission counter) was varied from 12 in. to 114 in. from the pion scattering target. The variable delay (see Fig. 2) was changed with the position of counter 4 to compensate for the pion time of flight. The positions of counter 4 were chosen to obtain conveniently spaced data points on both the diffraction and absorption portions of the measured cross-section curve, $\sigma_m(\theta)$.

In poor geometry, target thicknesses were chosen to give approximately 10% attenuation. In good geometry, targets were made as thick as possible, consistent with small multiple-scattering corrections. Target thicknesses and angles subtended by counter 4 are listed in Table I. The transmission counter, counter 4, was used in anticoincidence with respect to the monitor counters, counters 1, 2, 3. (See Sec. II, D.)

B. Pion Beam

The (442 ± 8)-Mev positive-pion beam was produced by the regenerated 740-Mev proton beam, from the Berkeley synchrocyclotron, impinging on an external carbon target. The pion beam was partially momentum-analyzed by a wedge-focusing magnet whose pole tips were designed to give equal horizontal and vertical foci at the position of the second bending magnet. A 4-in.-

TABLE I. Measured attenuation cross sections as a function of transmission counter angle, and corrections to the measurements.

Element	Thickness (g/cm^2)	θ (radians)	Measured $\sigma_m(\theta)$ cross section (mb)	$\delta\sigma_m$ Statistical counting error (mb)	Multiple Coulomb correction (mb)	Estimated multiple Coulomb correction error (mb)	Measured $\sigma_m(\theta)$ corrected for Coulomb (mb)	$\sigma_m(\theta)$ measured corrected for Coulomb, accid. muons (mb)
C	4.981	0.0519	351.8	± 9.1	18	±13	334	355±16
C	6.821	0.0608	325.2	± 6.2	6	±4	319	339±7
C	6.821	0.0846	309.5	± 5.3	2	±2	308	327±6
C	11.802	0.1894	245.6	± 3.7	0	0	246	261±4
C	11.802	0.2745	210.6	± 3.6	0	0	211	224±4
C	11.802	0.4236	166.0	± 3.2	0	0	166	176±3
Al	2.532	0.0522	756.7	± 34.1	65	±47	692	735±55
Al	3.369	0.0612	687.6	± 20.6	23	±18	665	706±27
Al	6.753	0.0848	624.4	± 11.9	3	±2	621	660±12
Al	11.776	0.1920	445.3	± 8.0	0	0	445	473±8
Al	11.776	0.2798	354.2	± 6.4	0	0	354	376±6
Al	11.776	0.4361	295.9	± 6.4	0	0	296	314±6
Cu	2.807	0.0612	1536	± 58	144	±75	1392	1478±95
Cu	4.278	0.0706	1439	± 39	92	±38	1347	1431±54
Cu	5.655	0.0855	1264	± 29	27	±13	1237	1314±32
Cu	16.931	0.1949	778.5	± 13.2	0	0	779	827±13
Cu	16.931	0.2862	666.9	± 12.0	0	0	667	708±12
Cu	16.931	0.4511	562.1	± 11.2	0	0	562	597±11
Cd	2.078	0.0612	2717	±131	418	±192	2299	2442±233
Cd	2.803	0.0706	2432	± 92	231	±101	2201	2337±137
Cd	4.189	0.0855	2023	± 61	86	±37	1937	2057±71
Cd	13.903	0.1955	1121	± 24	0	0	1121	1191±24
Cd	13.903	0.2871	970	± 22	0	0	970	1030±22
Cd	13.903	0.4536	816	± 20	0	0	816	867±20

thick carbon "energy degrader," inserted in the opening to the channel through the shielding wall, greatly reduced proton contamination of the pion beam reaching the detectors. The momentum of the transmitted protons differed from that of the pions enough that the protons could be rejected by the second bending magnet. A Čerenkov counter in the beam-monitoring circuit precluded the detection of the few remaining protons.

Currents in the three-element, 4-in.-bore quadrupole magnet were adjusted to obtain equal horizontal and vertical foci at approximately 20 ft from the quadrupole, the greatest distance at which the transmission counter was placed.

The optimum pion flux of 500 π^+/min passing through counters 1, 2, and 3 was obtained using a 4-in.-thick carbon production target.

The pion beam energy and energy spread were obtained from analysis of range curves (Fig. 3) of the proton beam admitted by removal of the carbon block and Čerenkov counter. A range curve for positive pions

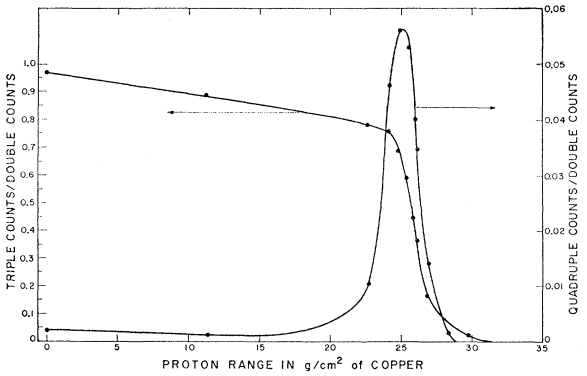

FIG. 3. Integral and differential proton range curves used to determine the momentum acceptance band of the magnetic system.

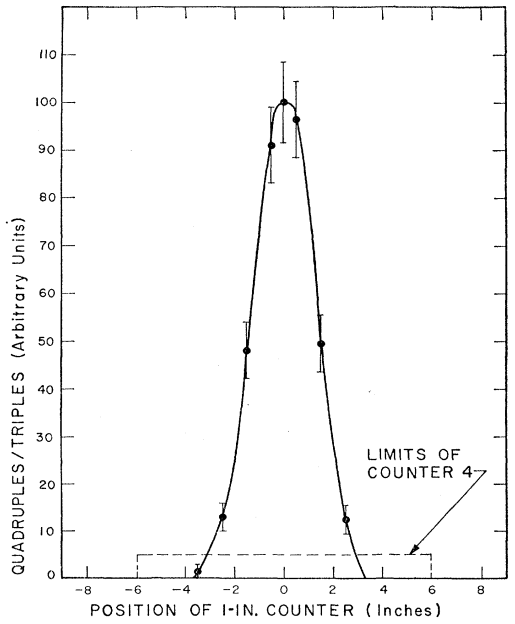

FIG. 4. Beam profile taken at 115 in. from the target position with a 1-in.-diam counter.

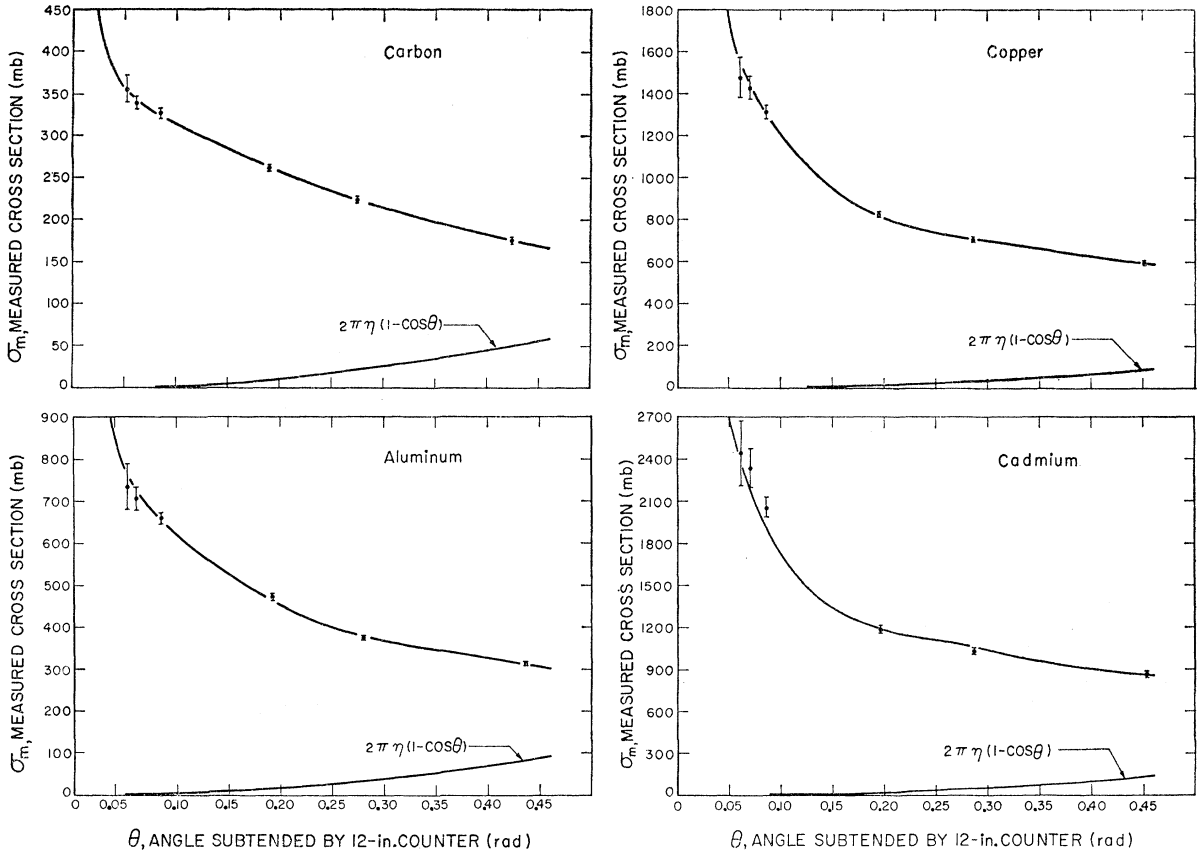

FIG. 5. The measured pion cross section on carbon, aluminum, copper and cadmium, as a function of the angle subtended by the 12-in. counter. The experimental points are the corrected cross sections from Table I. The two lines are $\sigma_m(\theta)$ and $2\pi\eta(1-\cos\theta)$ from Eq. (3) for the best fit.

at 390 Mev was used to ascertain the muon contamination. The measured muon contamination was corrected for multiple Coulomb scattering losses[6,7] in traversing the thick copper absorber, and for pion decay in flight after the second bending magnet. Muon contamination was found to be $(4.0\pm1.5)\%$ at 390 Mev. Calculation shows that the muon contamination at 390 Mev is the same as that at 442 Mev, within the error given above. The electron contamination was estimated to be negligible by calculation.

C. Beam Profile

The fraction of the beam particles that miss counter 4 due to multiple Coulomb scattering for a given target thickness and a given counter-4 distance is rapidly reduced as the beam profile is narrowed. To make multiple Coulomb scattering corrections, an accurately known beam profile is essential. Beam profile width was minimized by quadrupole focusing and by requiring the beam to traverse counter 3 (1.5-in. diam). Figure 4 shows the beam profile at 115 in. from the target ($\theta=0.052$ rad for counter 4) as measured by translating a 1-in.-diam counter across the beam. In addition to this, beam intensity measurements in concentric rings about the beam axis were made by varying the position of different diameter circular counters along the beam axis. Coulomb corrections were based mostly on the latter measurements as they were more accurate than those taken with the 1-in.-diam counter.

D. Counters and Electronics

Figure 2 is a block diagram of the electronic circuits used. The monitor counters were a 4-in.×4-in.×2-in.-thick water-filled Čerenkov counter (counter 1) and two $\frac{1}{4}$-in.-thick plastic scintillators of diameters 2 in. and $1\frac{1}{2}$ in. (counters 2 and 3). Counts due to pions scattered at angles less than θ were electronically rejected by pulses coming from a 12-in.-diam, 1-in.-thick plastic scintillator (counter 4). The response over the surface of counter 4, as tested with a radioactive β source, was found to be uniform within ±25 v on the photomultiplier high-voltage supply. Operation of counter 4 at 50 v above minimum plateau assured uniformity of response over the face of the counter. The efficiency of counter 4 was greater than 99%. RCA 6810 phototubes were used for all counters. All counters were

[6] R. M. Sternheimer, Rev. Sci. Instr. 25, 1070 (1954).
[7] L. Eyges, Phys. Rev. 74, 1534 (1948).

clamped to an I-beam which was accurately aligned with the pion beam by beam profile measurements with a 1-in.-diam counter (see Fig. 4).

Use of the 4-in. carbon block previously mentioned reduced the proton-to-pion ratio from 20/1 to 3/1. Due to the low duty cycle of the cyclotron, the reduction of beam contamination by protons was desirable to preclude jamming of counter 4.

III. RESULTS

Table I presents the measured and corrected cross sections as a function of angle.

Cross sections and statistical counting errors were calculated on the basis of the relations

$$\sigma_m=\frac{1}{Nt}\ln\left(\frac{I}{I_0}\right)=\frac{1}{Nt}\ln\left(\frac{1-Q_0/T_0}{1-Q_i/T_i}\right), \quad (1)$$

$$[(\delta\sigma_m)^2]^{\frac{1}{2}}=\frac{1}{Nt}\left[\frac{Q_i/T_i^2}{(1-Q_i/T_i)^2}+\frac{Q_0/T_0^2}{(1-Q_0/T_0)^2}\right]^{\frac{1}{2}}, \quad (2)$$

where N is the number of nuclei per cm^3, t is the target thickness in cm, T_i and T_0 are the triple coincidences 123 with target in and out, respectively, and Q_0 and Q_i are quadrupole coincidences $123\bar{4}$.

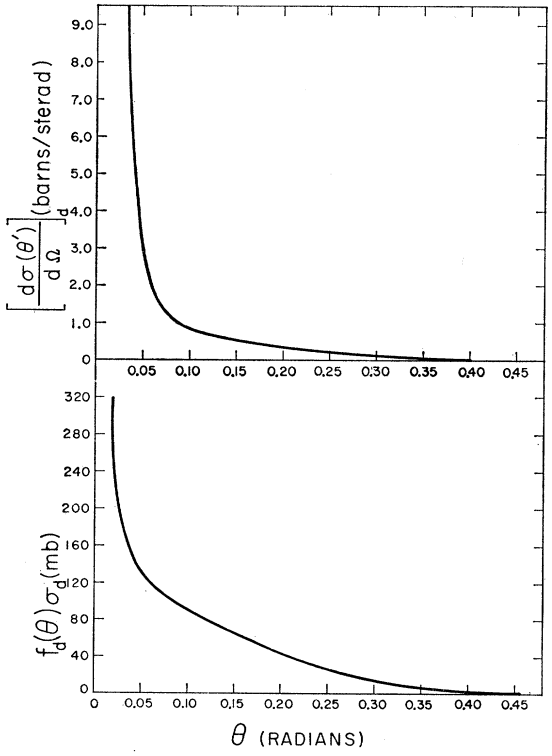

FIG. 6. The upper curve is $[d\sigma(\theta')/d\Omega]$ for carbon with $V_R=32.5$ Mev and $V_I=40$ Mev, as calculated by Loki. The lower curve is $f_d(\theta)\sigma_d$, calculated from Eq. (4) for carbon with $V_R=32.5$ Mev and $V_I=40$ Mev.

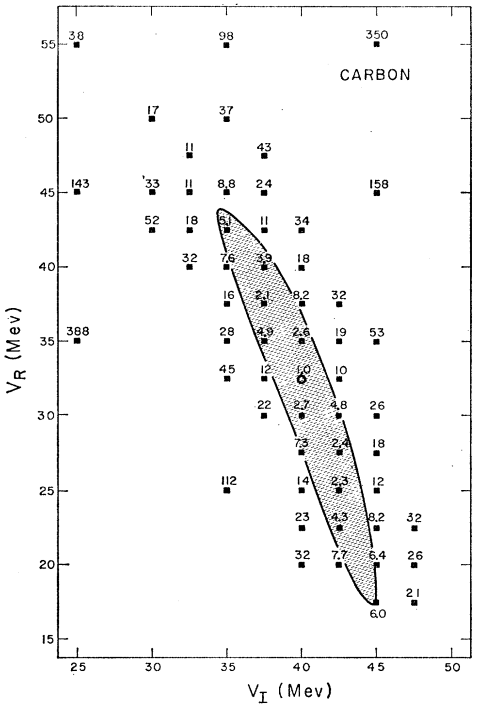

FIG. 7. Contour graph of S [see Eq. (5)] as a function of V_R and V_I for carbon. The solid curve represents the $S=6$ contour. The correct V_R and V_I pair should lie within the shaded portion.

The experimental points in Fig. 5 graphically present the corrected cross sections of Table I.

The measured cross section $\sigma_m(\theta)$ may be expressed[8] by the relation

$$\sigma_m(\theta)=\sigma_a+f_d(\theta)\sigma_d-2\pi\eta(1-\cos\theta), \quad (3)$$

where σ_a is the absorption cross section, σ_d is the diffraction cross section, η is the parameter which expresses the charged secondaries, and θ is the angle subtended by counter 4. The effect of the finite resolution is taken into account by

$$f_d(\theta)\sigma_d=2\pi\int_0^\pi\left[\frac{d\sigma(\theta')}{d\Omega}\right]_d R(\theta-\theta')\sin\theta' d\theta', \quad (4)$$

where $[d\sigma(\theta')/d\Omega]_d$ is the diffraction-scattering differential cross section and nuclear Coulomb scattering cross section, and $R(\theta-\theta')$ is the resolution function for the finite beam size.

To determine from the experimental measurements the values of V_R and V_I, we minimized the quantity

$$S=\sum_{i=1}^{6}[\Delta\sigma_m(\theta_i)]^{-2}\times[f_d(\theta_i)\sigma_d+\sigma_a-2\pi\eta(1-\cos\theta_i)-\sigma_m(\theta_i)]^2, \quad (5)$$

[8] J. W. Cronin, R. Cool, and A. Abashian, Phys. Rev. **107**, 1121 (1957).

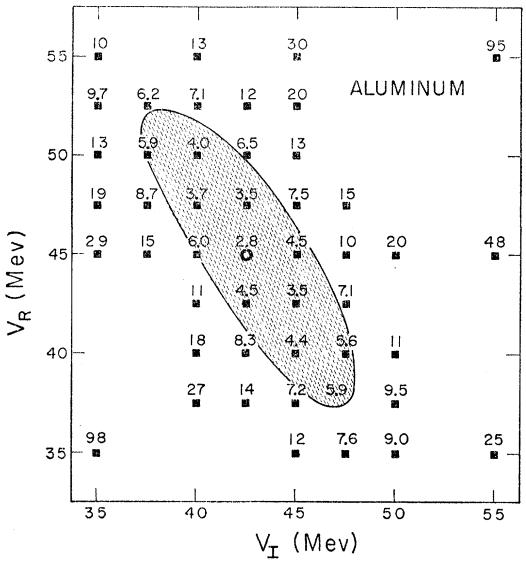

FIG. 8. Contour graph of S [see Eq. (5)] as a function of V_R and V_I for aluminum. The solid curve represents the $S=6$ contour. The correct V_R and V_I pair should lie within the shaded portion.

with respect to η, V_R, and V_I. The quantity $\Delta\sigma_m(\theta_i)$ is the error in the measured cross section tabulated in Table I.

Computations of σ_a, σ_d, and $[d\sigma(\theta')/d\Omega]_d$ were accomplished by an IBM 704 program named "Loki," which numerically integrated the radial component of the wave equation. The technique was similar to that used by Woods and Saxon.[9] The program treated pions relativistically, ignoring second order terms of potentials in the Klein-Gordon equation. The optical-model nuclear potentials were represented by

$$V(r)=-\frac{V_R+iV_I}{1+\exp[(r-r_0A^{\frac{1}{3}})/a]},$$

with $r_0=1.14\times10^{-13}$ cm and $a=0.45\times10^{-13}$ cm. Positive values of V_R and V_I mean repulsive potentials. The nuclear Coulomb potential was that due to a uniform spherical charge distribution of radius $r_0A^{\frac{1}{3}}$.

The upper half of Fig. 6 shows $[d\sigma(\theta')/d\Omega]_d$ for carbon with $V_R=32.5$ Mev and $V_I=40$ Mev; the lower half shows $f_d(\theta)\sigma_d$ obtained from Eq. (4).

Least-squares fitting to the experimental data was done by an IBM 650 program. For given pairs of V_R and V_I, S was minimized with respect to η to obtain the best value of S for each V_R and V_I pair. Contour graphs of S are shown as a function of V_R and V_I in Figs. 7–10. A minimum on these graphs denotes the best values of V_R and V_I for each target element. No fit for the cadmium data was obtained in the range of the V_I and V_R values used. The curves shown in Fig. 5 are $\sigma_m(\theta)$ for best fits [see Eq. (3)]. The quantity $2\pi\eta(1-\cos\theta)$ is also plotted to show the effect of charged secondaries.

The expected value of S equals the number of degrees of freedom, which is three in our case since we have measurements at six angles with three parameters to fit.

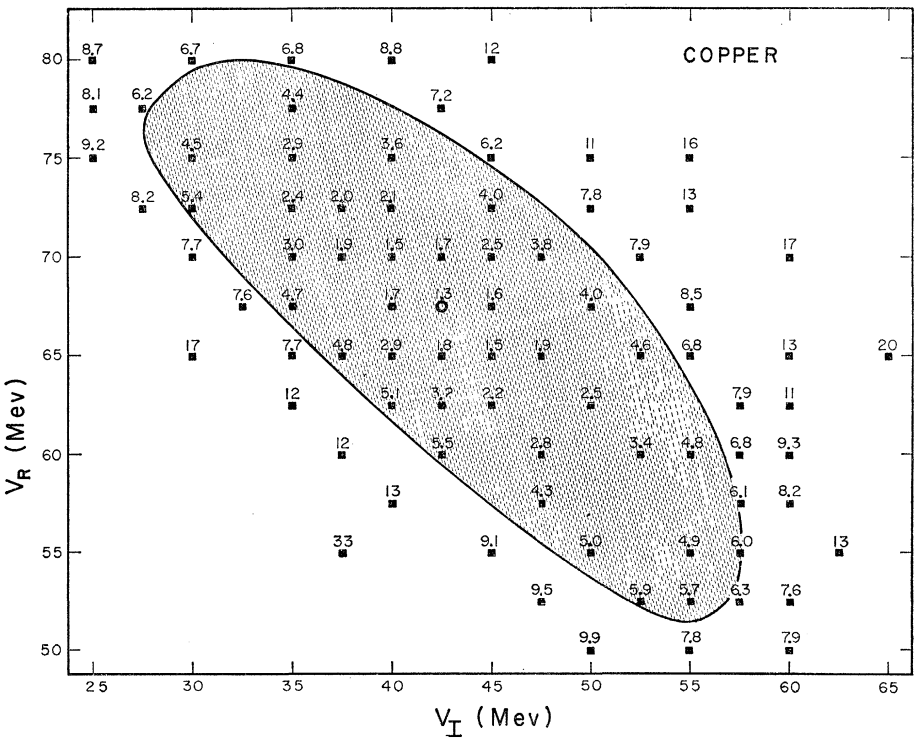

FIG. 9. Contour graph of S [see Eq. (5)] as a function of V_R and V_I for copper. The solid curve represents the $S=6$ contour. The correct V_R and V_I pair should lie within the shaded portion.

[9] R. D. Woods and D. S. Saxon, Phys. Rev. 95, 577 (1954).

TABLE II. The real and imaginary potentials and the absorption and diffraction cross sections. S is defined by Eq. (5), η by Eq. (3).

Element	S	η (mb/sr)	V_R (Mev)	V_I (Mev)	σ_a (mb)	σ_d (mb)
C	1.0	92±36	32.5±12	40±5	225±19	121±25
Al	2.8	141±44	45±7	42.5±5	387±24	351±35
Cu	1.3	137±98	67.5±12	42.5±13	648±100	942±165
Cd	8.2	212	75	25	754	1674

To estimate the errors in V_I, V_R, σ_a, σ_d, we used the contour graphs of S. The correct V_R and V_I should lie within the S ($=2S$ expected) $=6$ contour (see Figs. 7–9). The best-fit values and their estimated errors are listed in Table II.

IV. CORRECTIONS

The good-geometry data were corrected for multiple Coulomb scattering in the targets, while the poor-geometry data corrections were shown to be negligible. In making the corrections, we modified the method outlined by Sternheimer.[6] From the measured cross section we subtracted the quantity $(1/Nt)(1-F)$. F is given by

$$F=\int_0^{\rho_0'} n(\rho')f(\rho',r_0')\rho'd\rho' \Big/ \int_0^{\rho_0'} n(\rho')\rho'd\rho', \quad (6)$$

in which $n(\rho')$ is the density of particles per unit area on the transmission counter (counter 4) with the target removed; ρ' is the particle radius divided by the counter radius; r_0' is a function of the pion's energy, the thickness of the target in radiation lengths, and the distance of the transmission counter from the target[6]; $f(\rho',r_0')$ is the probability that the scattered pion strikes counter 4 for a given ρ' and r_0'. F was obtained by numerical integration using the IBM 650 computer. The correction values and their estimated errors are listed in Table I. The errors on the corrections are due mainly to indeterminacy in the measured beam shape, $n(\rho')$. We calculated the corrections using the maximum and minimum possible values of $n(\rho')$ to estimate the magnitude of the corrections.

The accidental correction was $\alpha=(2\pm1)\%$ for all runs. The muon correction was $\beta=(4.0\pm1.5)\%$. The corrected cross section is given in terms of the measured cross section by

$$\sigma_{(\text{corrected})}=\sigma_{(\text{measured})}(1+\alpha)/(1-\beta),$$

or

$$\sigma_{(\text{corrected})}=1.06\sigma_{(\text{measured})}.$$

V. DISCUSSION

With our limited amount of experimental data on the pion-nucleus cross sections, we did not think it feasible to attempt to determine all the parameters V_R, V_I, η, r_0, and a. Instead, we assumed that the distribution of nuclear matter in nuclei is approximately the same as the charge distribution, so the nuclear radius parameter r_0 and the falloff parameter a are determined.

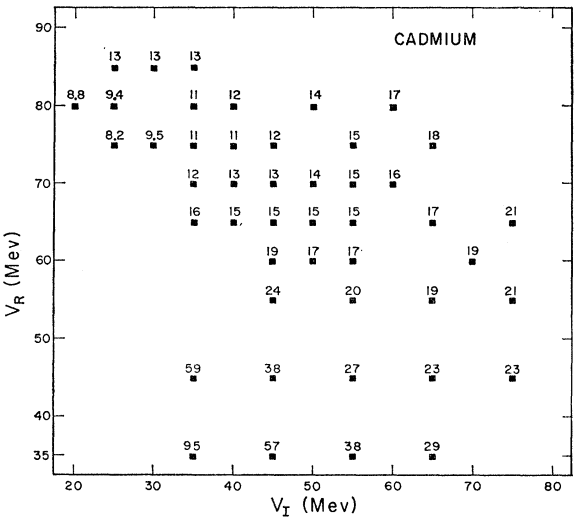

FIG. 10. Contour graph of S [see Eq. (5)] as a function of V_R and V_I for cadmium. No fit was obtained in the range of V_R and V_I values used.

Another limitation on the interpretation of the results of this experiment stems from the fact that in the "good" geometry measurement we had no experimental criterion to determine whether the scattering was indeed elastic. From differential scattering measurements performed at lower energies[10] and on theoretical grounds[11] there is sufficient evidence to indicate that the diffraction scattering is the dominant effect at small angles and that the inelastic contribution—the "quasi-elastic" and the "direct inelastic" scattering—becomes appreciable for angles θ greater than the first minimum. Since our good geometry measurements extended well into the first diffraction peak, we feel that it is justifiable to neglect the effect of the inelastic contributions.

The theoretical values for the optical-model potentials as calculated by Watson and Zemach[3] are $V_R=30$ Mev and $V_I=45$ Mev. The method used to calculate the cross sections from potentials was sensitive to the sign of the potentials because of the interaction between the nuclear and Coulomb terms. However, in our calculation only positive potentials were used and no attempt was made to fit the data with negative potentials. The experimental values for V_I are in fairly good agreement with the theoretical values, as can be seen from Fig. 11. However, experimentally V_R increases with increasing atomic number to values far above 30 Mev (see Fig. 11).

Actually one might expect some deviation for small A (atomic number), but the agreement should be better for large A where the assumptions of the optical model are more meaningful. Since our results give better

[10] R. M. Edelstein, W. F. Baker, and J. Rainwater, Phys. Rev. 122, 252 (1961).
[11] T. K. Fowler and K. M. Watson, Nuclear Phys. 13, 549 (1959).

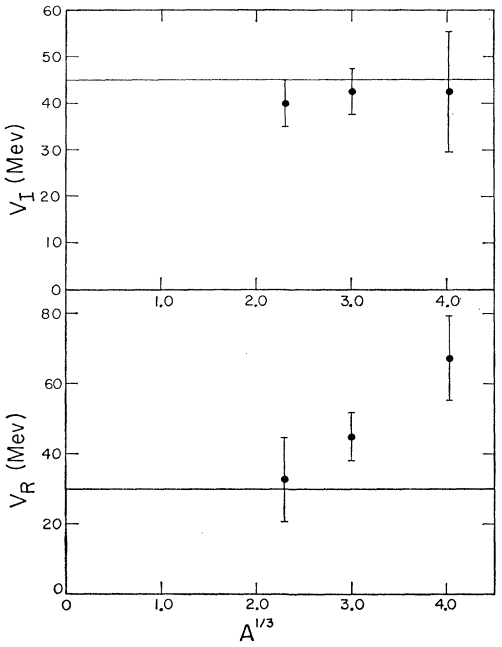

FIG. 11. The imaginary potential V_I and real potential V_R as a function of the cube root of the atomic number. The straight lines are the theoretical values from reference 3.

agreement for small A than large A, this indicates that perhaps a different r_0 and a could be found which would agree for the larger A elements. The values determined by electron scattering experiments are $r_0=1.08\times10^{-13}$ cm and $a=0.53\times10^{-13}$ cm. Due to an oversight on our part, the values that we used in our calculations to determine the experimental V_R and V_I were $r_0=1.14\times10^{-13}$ cm and $a=0.45\times10^{-13}$ cm. Using a smaller value for the radius in the calculations, however, would only be in a direction to give a larger experimental V_R value. The falloff parameter a has less effect on the potentials than r_0. Therefore, we believe the disagreement between the experimental and theoretical V_R would be as great or greater with the r_0 and a from electron scattering experiments.

In summary, if we accept the nuclear parameters as approximately those determined by charge distribution measurements, then the results suggest that the effective real pion-nucleus potential is greater than that predicted by theory.[3] If we assume the optical-model potentials are correct, the results indicate that there is a different pion-nucleus interaction volume than that of the charge distribution.

ACKNOWLEDGMENTS

We are pleased to acknowledge the continued interest of Professor A. C. Helmholz and to express our appreciation to Mr. James Vale and the cyclotron crew. The authors also wish to thank Dr. Sidney Fernbach, Dr. Joel Bengston, and Dr. Frank Bjorklund for invaluable discussions and extensive IBM 704 computations of the optical-model parameters.